

Article

Detailed Theoretical Characterization of a Transcritical CO₂ Direct Expansion Ground Source Heat Pump Water Heater

Parham Eslami-Nejad *, Messaoud Badache, Arash Bastani and Zine Aidoun

CanmetENERGY, Natural Resources Canada, 1615 Lionel-Boulet, Case Postale 4800, Varennes, QC J3X 1S6, Canada; messaoud.badache@canada.ca (M.B.), arash.bastani@canada.ca (A.B.), zine.aidoun@canada.ca (Z.A.)

* Correspondence: parham.eslaminejad@canada.ca; Tel.: +1-450-652-4894

Received: 30 November 2017; Accepted: 29 January 2018; Published: 7 February 2018

Abstract: A new avenue in modern heat pump technology is related to the use of natural refrigerants such as carbon dioxide (CO₂). The use of CO₂ in direct expansion ground source heat pumps (DX-GSHP) has also gained significant interest as it offers opportunities for cost reduction of the ground loop, albeit some challenges remain in their development, design and use. To address these challenges and to characterize CO₂-DX-GSHP performance for water heating applications, a detailed theoretical model and a fully-instrumented test apparatus was developed and built at CanmetENERGY Research Laboratory. The theoretical model was validated against a set of experimental results and adopted to investigate the performance of the system over a wide operating range. Validation results showed that the model predicts the experimental results within the measurement uncertainty. A detailed system performance analysis was also performed using the theoretical model to understand the system behavior and explore the actions required for performance improvement in future installations. The results of the analysis showed that improper design and control of some components, such as the gas cooler and ground heat exchanger can degrade the system performance by up to 25%, and the heat pump heating capacity by 7.5%.

Keywords: direct expansion ground source heat pump; CO₂; transcritical; parametric analysis; modeling

1. Introduction

In North America, Europe and China, ground-source heat pump (GSHP) systems have been installed more widely during recent years to provide heating and cooling for several applications. Being more energy efficient compared to the conventional air-source systems, such systems can offer reduced GHG emissions. GSHP systems can be divided into two categories, namely the secondary loop GSHP (SL-GSHP) and the direct expansion GSHP (DX-GSHP). In the former, the heat pump and the ground are generally connected by means of a closed loop where a heat-carrier fluid (water or a solution of antifreeze and water) flows and transfers heat from the soil to the refrigerant in the heat pump. Conversely in DX-GSHP systems, ground heat exchangers (GHE) or boreholes act as a condenser or evaporator, depending on the operation mode. In general, the performance of a GSHP system is influenced by many variables such as type of GHE, soil condition, local climate, building load characteristics, system design and control parameters [1–3].

Although many studies have been performed on the SL-GSHP and GHEs with single-phase heat carrier fluid, modeling of the DX-GSHP systems has been rarely studied.

Kruse and Russmann [4] and Bertsch et al. [5] proposed a ground heat pipe technology with two-phase CO₂ as a heat carrier fluid for extracting heat from the ground and transferring it to

the GSHP using the thermosyphon principle. Both studies used pipe-in-pipe configurations. They compared the proposed system with a conventional system using a single-phase water/brine solution.

Compared to the SL-GSHP, relatively few works have been published on the DX-GSHP, which mainly operates with R22 and R12 as the working refrigerant [6–12]. Fannou et al. [13], Wang et al. [14] and Mineas [15] investigated the possibility of replacing R22 with other refrigerants such as R410A, R134a and R407. They studied different types of GHE (horizontal, vertical, spiral and inclined) in the heating and cooling mode. Johnson [8] Mineas [15] and Goulburn [16] performed several studies on horizontal GHEs in heating mode. Inclined GHEs have been investigated by [17,18]. Kim et al. [19] evaluated a direct expansion vertical closed-loop ground source heat pump for residential application. A system using spiral copper GHE buried in three 17 m trenches has been built and tested by Lenarduzzi and Bennett [20]. Some research has investigated the performance of the entire system experimentally using common refrigerants [14,21], while others have focused on simulation and modeling the complexity of two-phase flows in the ground heat exchanger [11,12,22,23]. Safemazandarani et al. [24] introduced the first mathematical model of a direct expansion ground-coupled heat pump system. After that, Beauchamp et al. [25] developed a transient GHE model that was refined in [18] and presented in [11]. However, the authors did not consider gravity in the void fraction model. Fannou et al. [12] studied the heating capacity and the coefficient of performance (COP) of a vertical DX-GSHP using an artificial neural network method. In this research, the authors focused on the execution of the best control strategies of the DX-GHP operation. Rousseau et al. [22] presented a numerical model for evaluating the transient behavior of a vertical U-tube direct-expansion ground heat exchanger performance using R-22 as the refrigerant. They analyzed the effects of mass flow rate, the length and the angle of the borehole on the heat flux rate. Moreover, Halozan and Rieberer [26] evaluated the commercialization of DX-GSHP and the barriers facing the technology. Guo et al. [27] carried out a techno-economic study to compare DX systems with secondary loop (SL) systems in cooling mode. Hakkaki-fard et al. [28] made a techno-economic comparison of a DX-GSHP and an air-source heat pump system in the Canadian cold climate. Two comprehensive reviews of DX-GSHP systems have been presented by [29,30].

Regarding CO₂ as the refrigerant, Mastrullo et al. [31] numerically modeled a CO₂-filled U-tube ground heat exchanger (borehole) under thermosyphon principles for the secondary loop GSHP systems. The authors investigated the effect of two main parameters: fluid flow rate and borehole inlet temperature. Eslami-Nejad et al. [32] focused on the numerical modeling of CO₂-filled U-tube vertical boreholes under forced circulation mechanism. Recently, refs. [33,34] studied DX-GSHP operating with CO₂ as the refrigerant. The former developed a mathematical model of the buried pipe using an energy balance method. The important factors such as the shank spacing, the thermal conductivity of soil and backfill material, the inlet temperature and the mass flow rate of the refrigerant were studied. In the latter study, a numerical model was developed to evaluate the performance of CO₂ GSHP with a horizontal ground heat exchanger for space heating and domestic hot water production. They conducted two separate parametric studies: one with a fixed GHE length and another with a constant heating load.

Very few works have looked at the entire CO₂ GSHP cycle. Austin and Sumathy [35] simulated a simple CO₂ transcritical cycle to analyze the performance of a CO₂ GSHP with a horizontal geothermal evaporator. However, they did not account for the dynamic characteristics of the system. Eslami-Nejad et al. [36] developed a quasi-transient CO₂ transcritical ground source heat pump model along with numerical and experimental validation of the borehole section. Recently, the research work by Badache et al. [37] experimentally investigated the CO₂ evaporation inside the ground heat exchanger and the effect of the number of active borehole on the overall performance of a DX CO₂ GSHP.

In the present study, the model from Eslami Nejad et al. [36] was adopted, improved and validated using a set of experiments carried out at CanmetENERGY Research Laboratory. It was then employed to conduct a parametric analysis on a DX CO₂ GSHP.

2. System Description

Figure 1 shows a schematic of a single-stage transcritical CO₂ DX-GSHP system with the hot gas bypass working in heating mode. The system consists of eight main system components including the compressor (1–2), gas cooler (2–3), internal heat exchanger (3–4), two different expansion valves (4–5 and 6–7), pressure regulating valve (9–10), receiver (5–6) and boreholes (7–8).

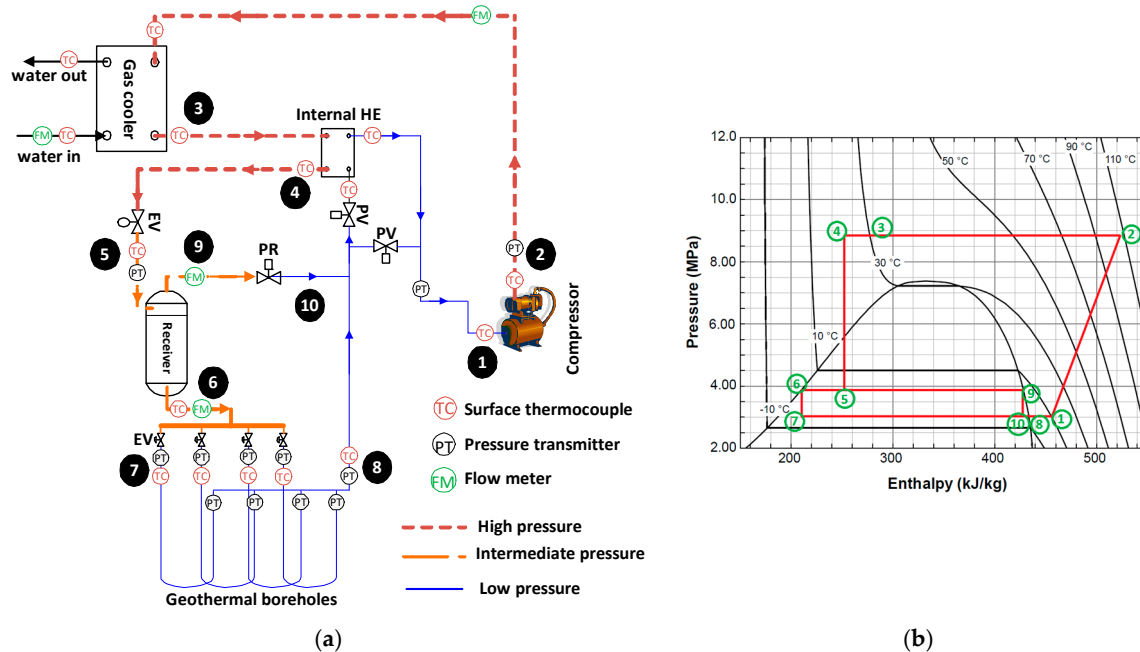


Figure 1. (a) System schematic; (b) Cycle P-h diagram.

2.1. Thermodynamic Cycle

As shown in Figure 1a, CO₂ (refrigerant) is flowing through a complete cycle by going directly down to the borehole, changing direction at the bottom (U connection) and coming up to extract heat ($q_{borehole}$) from the ground by evaporation (7–8, Figure 1b). It then enters the internal heat exchanger (IHE) to exchange heat with the gas at the gas cooler exit in order to be superheated to a certain degree (point 1, Figure 1b). The compressor then compresses the gas to the high-pressure level (supercritical pressure here at point 2, Figure 1b) with a corresponding temperature rise. The high pressure/high temperature vapor enters the gas cooler to heat the water (q_{gc}). After the IHE (point 4, Figure 1b), low temperature/high pressure CO₂ gas is throttled to the intermediate-pressure level of the cycle (point 5, Figure 1b). Two-phase CO₂ (vapor and liquid) enters the receiver (known as a separator) and the vapor part is bypassed around the boreholes. Both liquid and vapor parts are throttled to the low-pressure level of the cycle (points 7 and 10, Figure 1b). Finally, CO₂ with low vapor quality enters the boreholes and mixes with bypassed vapor at the borehole outlet.

2.2. Test Bench

In an attempt to develop expertise on operating this type of system and to address recent challenges of using natural refrigerant in heat pumps, an experimental test bench was built at CanmetENERGY Research Laboratory. The test facility comprises the main components described above. Two counter-flow plate heat exchangers were used for the gas cooler ($A_{gc} = 0.74 \text{ m}^2$ and $UA_{gc} = 0.3 \text{ kW/K}$ at test conditions) and for the IHE ($A_{IHE} = 0.092 \text{ m}^2$ and $UA_{IHE} = 0.1 \text{ kW/K}$ at test conditions). The heat pump is connected to four 30m vertical boreholes with single copper U-tube arranged in a square pattern with a uniform spacing of 6.25 m. Compressor characteristics and borehole

dimensions are listed in Tables 1 and 2, respectively. In situ thermal properties of the soil obtained from a thermal response test are given in Table 3.

Table 1. Semi hermetic compressor.

Compressor	Nominal refrigeration capacity	ton	1
	Nominal power input	kW	1.36
	Displacement at 60 Hz	m ³ /h	1.12

Table 2. Borehole dimensions.

Borehole	r_{borehole}		cm	3.9
	U	ID		0.64
		OD		0.8
	D	ID		0.48
		OD		0.64
	2D			2.3
	k_{grout}		W/m/K	0.8
	k_{pipe}			400
	Length		m	30

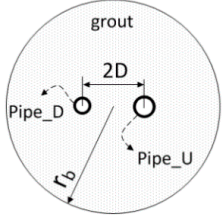


Table 3. Ground thermal properties.

Ground	k_{ground}	W/m/K	2.65
	$(\rho c_p)_g$	kJ/m ³ /K	2862
	T_{ground}	°C	9.0

As shown in Figure 1, the setup is fully equipped with different measuring devices including pressure and temperature sensors and flow meters to precisely measure the overall system performance as well as components of the cycle. The system can be operated in two different modes; automatic and manual. The automatic mode is employed in this paper and it is described in the following section. In the manual mode, the opening position of the expansion valves installed before the inlet of the boreholes can be changed manually.

2.2.1. Operating Controls

In the automatic mode, four main control strategies are applied as follow:

1. The valve that discharges the vapor from the receiver (identified PR in Figure 1a) maintains the intermediate pressure (P_{receiver}) at 3750 kPa. This value is the set point given by the operator that corresponds to a CO₂ saturation temperature of 2.8 °C.
2. The expansion valve installed after the IHE controls the discharge pressure of the compressor (high-pressure level). The control system follows an equation giving the optimum pressure (P_{opt}) set by the manufacturer in kPa as a function of gas cooler outlet temperature ($T_{\text{gc,out}}$) in °C.

$$P_{\text{opt}} (T_{\text{gc,CO}_2}) = 150 \times T_{\text{gc,out}} + 2600 \quad (1)$$

3. The opening of the expansion valves changes automatically to be able to provide superheat temperature set point (1.5 °C) at the borehole exit.
4. Two valves installed at the low-pressure level before the IHE (identified PV in Figure 1a) satisfy the second superheat set point (5.0 °C) at the compressor suction by modulating the flow of CO₂ passing through the IHE.

3. Theoretical Model

The system presented in Figure 1 was modeled using steady-state coupled enthalpy-pressure-heat transfer models of the borehole and gas cooler, a transient analytical model of the ground and steady-state heat transfer and thermodynamic models of other components such as the expansion valves, the pressure regulating valve, the compressor, the IHE and the receiver. The detailed description of the model including the pressure drop and heat transfer correlations for CO₂ evaporation and gas cooling has been provided in reference [36]. Short descriptions of the model components are listed in Table 4.

Table 4. Summary of the theoretical model.

Components	Model	Description	References
Borehole	Numerical steady-state coupled pressure, enthalpy and heat transfer model	Includes quasi-3-dimensional heat transfer in the GHE based on the 2-dimensional thermal resistances proposed by Hellström [38] for pipe and grout and perpendicular 1-dimensional coupled energy conservation and pressure drop equations for two-phase CO ₂ evaporation.	Eslami-Nejad et al. [32]
Soil	Transient classical finite line source (FLS) heat transfer model	Includes heat transfer in the soil (homogeneous medium) as well as the thermal interaction between boreholes with the heat pulse response superposition in time using a non-history scheme.	Lamarche and Beauchamp [39]
Gas cooler	Numerical steady-state coupled enthalpy-pressure-heat transfer models	Includes coupled heat transfer and pressure drop equations based on the finite volume approach for pipe-in-pipe heat exchanger.	Eslami-Nejad et al. [36]
Compressor	Steady-state	Includes single node model based on thermodynamic principles and given volumetric and isentropic efficiency relations.	
Internal heat exchanger	Steady-state	Includes single node heat transfer model based on effectiveness-NTU method	
Expansion and pressure regulating valves	Steady-state	Includes single node energy conservation equation based on isenthalpic process	
Receiver (separator)	Steady-state	Includes single node energy conservation equation for separating liquid and vapor phases.	

3.1. Solution Procedure

At each time step, three main iterative numerical procedures, as well as several internal iterative calculation loops, were used to determine the operating conditions of the system components as well as the ground thermal condition for the next time step. The first loop calculates the borehole inlet pressure and mass flow rate that corresponds to the fluid conditions exiting the expansion valves located before inlet of the boreholes. This is the main loop that confirms that the first point of the cycle is on the last point and the thermodynamic states of all components are calculated using this loop. The second loop calculates the discharge pressure and outlet gas cooler temperature that satisfies both the control function and the heat transfer characteristics of the gas cooler. In the last iterative loop, the borehole wall temperature is updated, using the transient heat transfer calculation in the ground. Based on the convergence criteria for each loop, all three main loops interact iteratively until they all converge. The code is developed in FORTRAN, to which REFPROP Version 9.1 subroutines [40] are linked, to calculate the thermodynamic properties of CO₂ and water. More details about different components and the flow diagram of the solution procedure are presented in Eslami-Nejad et al. [36].

3.2. Model Validation

Uncertainties for the measured parameters are presented in Table 5. The uncertainty of temperature measurement can be as high as 0.8 °C (for measuring high temperatures) due to the use of pipe surface thermocouples. Temperature uncertainties due to heat losses from the pipe surface to the ambient and the thermal contact resistance between the thermocouples and the pipe surface are not taken into account.

Table 5. Measurement uncertainties.

Measured Parameters	Equipment	Uncertainty
Temperature	T-type thermocouples	$\pm 0.5\text{ }^{\circ}\text{C}$
CO ₂ mass flow rate	Coriolis flowmeter	$\pm 0.2\%$
Water mass flow rate	Magnetic flowmeter	$\pm 0.5\%$
Pressure	Transducers	$\pm 0.6\%$
Power input to the compressor	Wattmeter	$\pm 0.2\%$

There are differences between the theoretical model and the test bench, including a separate expansion valve for each borehole and an oil circuit in the test bench but neither of these were considered by the model. A 17-h experiment was performed in heating mode for model validation with constant water mass flow rate (\dot{m}_{water}) entering the gas cooler at 0.025 kg/s and constant inlet water temperature at 35 °C. As shown in Figure 2, the CO₂ pressure value reaches over 8000 kPa at the gas cooler inlet as the high-pressure level is controlled based on Equation (1). Furthermore, intermediate pressure ($P_{receiver}$) is very close to the low pressure ($P_{in_borehole}$) level at 3750 kPa and 3540 kPa, respectively. Evaporating pressure ($P_{in_borehole}$) decreases slightly over time from 3540 kPa to 3412 kPa; this is caused by the expansion valves to maintain the superheat set point (1.5 °C) at the borehole outlet. Water temperature increases by 3.5 °C (from 35 °C to 38.5 °C) by taking the heat from CO₂ in the gas cooler (q_{gc}) and corresponding to nearly 3.6 kW of heating.

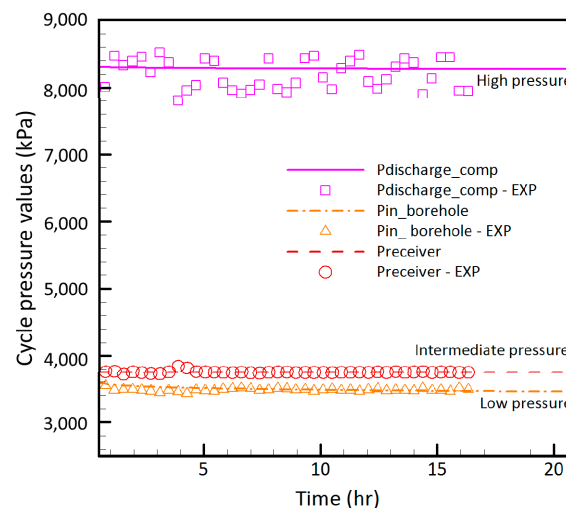


Figure 2. Cycle pressure levels.

The model originally developed by Eslami-Nejad et al. [36] was modified to include the four control strategies described in Section 2.2.1. Moreover, at the test conditions, certain dimensions were calculated for the pipe-in-pipe heat exchanger to have the same overall heat transfer coefficient as that of the plate heat exchanger used in the test bench (values are reported in Section 2.2). Figures 2 and 3 present the pressure levels of the heat pump and water and CO₂ temperatures of the gas cooler simulated by the model (lines) and measured (symbols) using the test bench. As these parameters together with the set points, control parameters and CO₂ thermodynamic properties are adequate to characterize the heat pump heating capacity and coefficient of performance. As such, these were selected for model validation. For instance, the heating capacity of the heat pump can be calculated experimentally based on the water mass flow rate and water temperature difference across the gas cooler. Similarly, the heat extraction from the soil is calculated experimentally using the inlet enthalpy to the borehole, evaporating pressure ($P_{in_borehole}$) and the superheat set point at the borehole outlet. As shown in Figures 2 and 3, the simulation results agree well with the experimental data within the

uncertainties of the measuring devices. Some experimental data was chosen arbitrarily (blue solid circles) to show error bars associated with the uncertainties reported in Table 5.

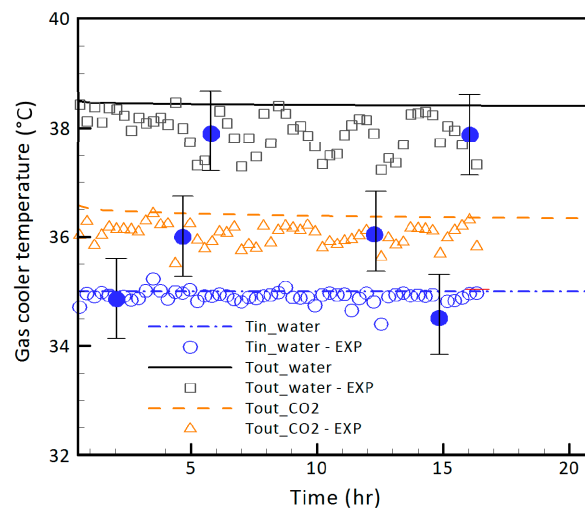


Figure 3. Gas cooler temperatures.

4. Application

For a better understanding of the system and to explore the actions required for performance improvement, a detailed performance analysis was undertaken using the theoretical model. This analysis focused on producing domestic hot water using the DX CO₂ GSHP (water temperature over 50 °C). Eight different cases were considered to be compared against the base case. A combination of the two best cases (#5 & #1) was also investigated in (#9). Two additional cases (BC2 and BC4) were also considered to investigate the effect of the number of boreholes. All system parameters that were different from those of the base case are presented in Table 6. One by one each parameter was changed in isolation for each case (#1 to #8, BC2 and BC4) to evaluate the effect of the seven following parameters: the degree of superheat at the compressor suction (ΔT_{sh_comp}), inlet water temperature to the gas cooler (T_{in_water}), CO₂ gas cooler outlet temperature (T_{out_CO2}), intermediate pressure ($P_{receiver}$), water mass flow rate (\dot{m}_{water}), IHE efficiency (ϵ_{IHE}) and number of boreholes in GHE. To solely investigate the effect of one parameter at a time, the optimum pressure control was not adopted here for the parametric analysis and the CO₂ outlet temperature from the gas cooler was fixed. Superheat controls at the borehole outlet and at the compressor suction were combined here into one control at the compressor suction and the entire CO₂ flow goes through the IHE. For the parametric study, the gas cooler was a co-axial countercurrent heat exchanger with a total length of 15 m and the cross section is presented in Figure 4. The overall heat transfer coefficient (U) of the gas cooler varied from case to case and with the evaporating temperature due to changes in CO₂ mass flow rate and properties (UA_{gc} changes from 0.12 to 0.3 kW/K).

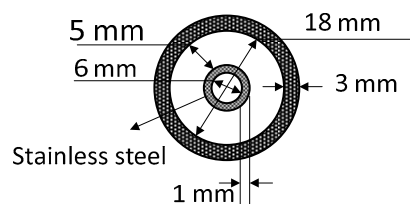


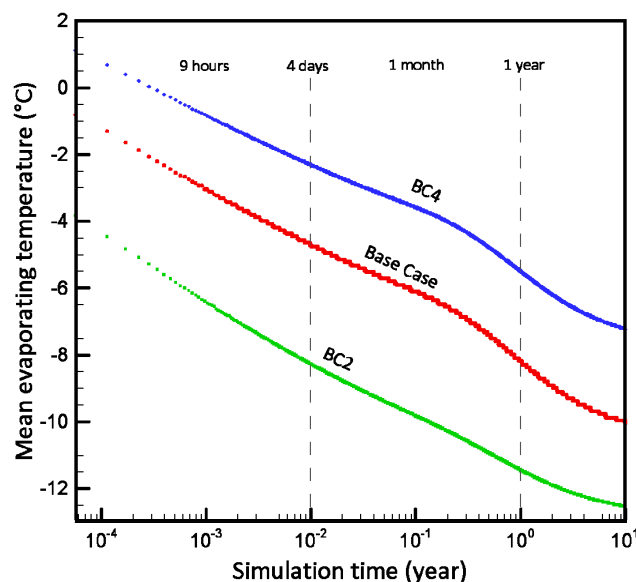
Figure 4. Gas cooler cross section.

Table 6. Different cases for parametric analysis.

Base Case					Other Cases	
Boreholes	U & D	ID	cm	0.64	#1	T_{out_CO2} 25 °C
		OD	cm	0.8	#2	T_{in_water} 25 °C
	k_{grout}		W/m/K	1.0	#3	ΔT_{sh_comp} 10 °C
	Length		m	3×30	#4	ΔT_{sh_comp} 1 °C
	T_{ground}		°C	9.0	#5	\dot{m}_{water} 0.03 kg/s
Gas cooler	\dot{m}_{water}		kg/s	0.025	#6	\dot{m}_{water} 0.02 kg/s
	T_{in_water}		°C	20	#7	$P_{receiver}$ 3578 kPa
	T_{out_CO2}		°C	30	#8	ε_{IHE} 10%
Other	ΔT_{sh_comp}		°C	5.0	#9	\dot{m}_{water} 0.03 kg/s
	$P_{receiver}$		kPa	4500		T_{out_CO2} 25 °C
	ε_{IHE}			40%	BC2	borehole 2×30
					BC4	borehole 4×30

4.1. Result Presentation

Simulation results summarize the detailed system characterization by presenting the effects of several parameters on COP, gas cooler heating capacity, compressor-work, discharge pressure, water outlet temperature, total borehole extraction rate and borehole pressure drop over the mean evaporating temperature. The evaporating temperature of the heat pump during operation depends on the amount of heat extracted from the soil over time, borehole performance and the soil thermal response. A relatively wide range is presented here for the mean evaporating temperature that corresponds to the transient behavior of the system during 10+ years. For instance, the evaporating temperature drops from the initial value to -8 °C, -5.5 °C and -11.5 °C after one year of continuous operation for the base case, BC4 and BC2, respectively (Figure 5). For other cases, the evaporating temperature values are between those of the BC2 and BC4 presented in Figure 5.

**Figure 5.** Mean evaporating temperature.

4.2. The Effect of Water Mass Flow Rate

The effect of water mass flow rate was studied in cases #5 and #6. As shown in Figure 6, among the cases from #1 to #8, for evaporating temperatures from -6 °C to 0 °C, the highest and the lowest COP were presented by case #5 ($\dot{m}_{water} = 0.03$ kg/s) and case #6 ($\dot{m}_{water} = 0.02$ kg/s), respectively. For instance, at 0 °C evaporating temperature, case #5 offers up to 8% higher COP than the base case.

On the other hand, reducing the water mass flow rate (case #6) significantly reduces the system COP by 15% at evaporating temperature of 0 °C in comparison with the base case. This is due to the fact that under the same CO₂ gas cooler outlet temperature the discharge pressure is significantly lower for case #5 compared to case #6 (Figure 7). However, as shown in Figure 8, gas cooler heating capacity in case #5 and #6 differs slightly from the base case. Borehole extraction rate in case #5 shows a slight difference from the base case, while in case #6, it is 6% lower than that of the base case (Figure 9).

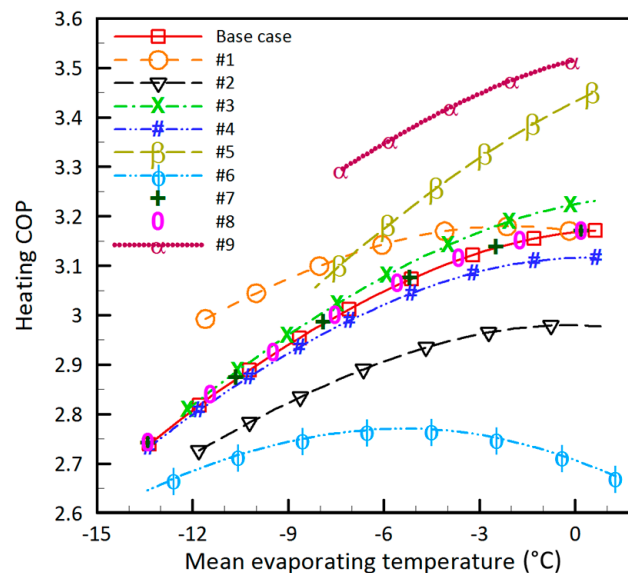


Figure 6. Coefficient of performance ($COP_{heating}$).

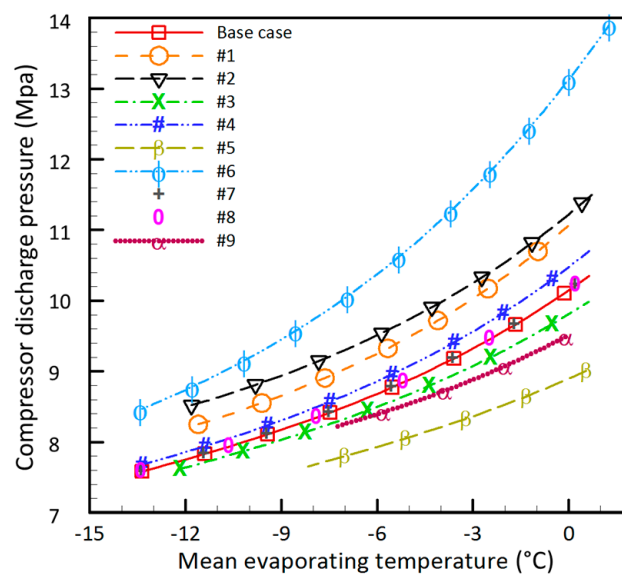


Figure 7. Discharge pressure ($P_{discharge_comp}$).

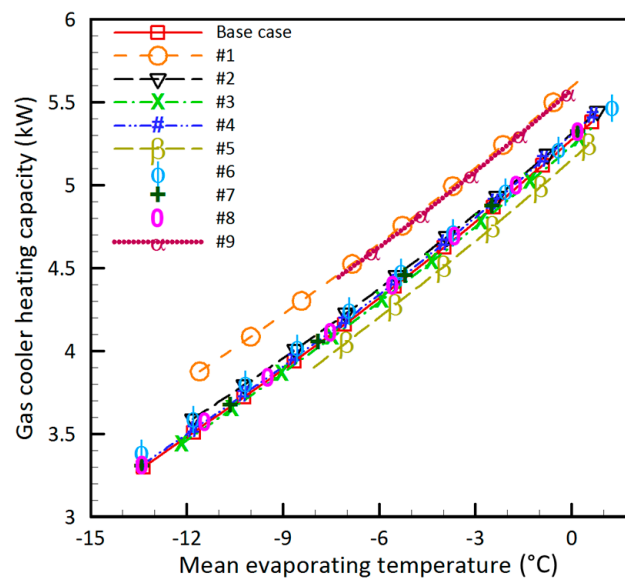


Figure 8. Gas cooler heating capacity (q_{gc}).

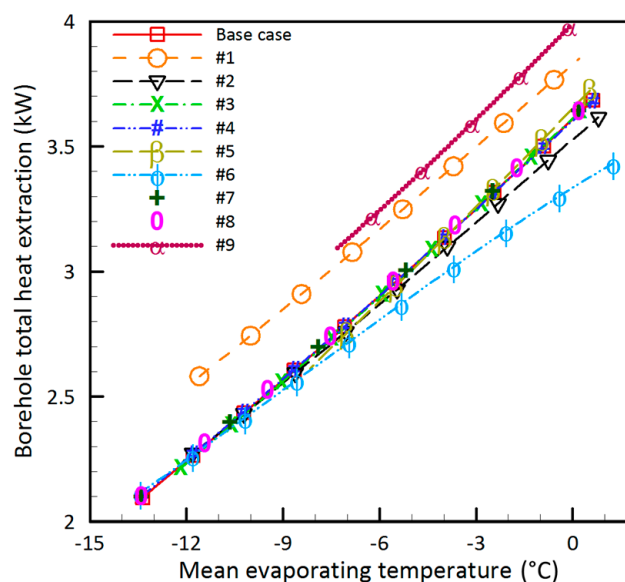


Figure 9. Total borehole extraction rate.

4.3. The Effect of CO₂ Gas Cooler Outlet Temperature

Reducing the CO₂ outlet temperature of the gas cooler (case #1) positively influences COP, particularly at low evaporating temperatures (up to 6% at −12 °C). The gas cooler heating capacity improves because of the increase in the discharge pressure (Figure 7). Meanwhile, the compressor work increases (Figure 10) to discharge CO₂ at a higher pressure. This is mainly due to the superior gas cooler performance at specific pressure and temperature conditions. Reducing the gas cooler outlet temperature also increases the liquid CO₂ mass flow rate into the boreholes and consequently enhances the total borehole extraction rate. Together with the higher work of the compressor and the higher gas cooler heating capacity, the water outlet temperature increases for the whole range of evaporating temperature (Figure 11).

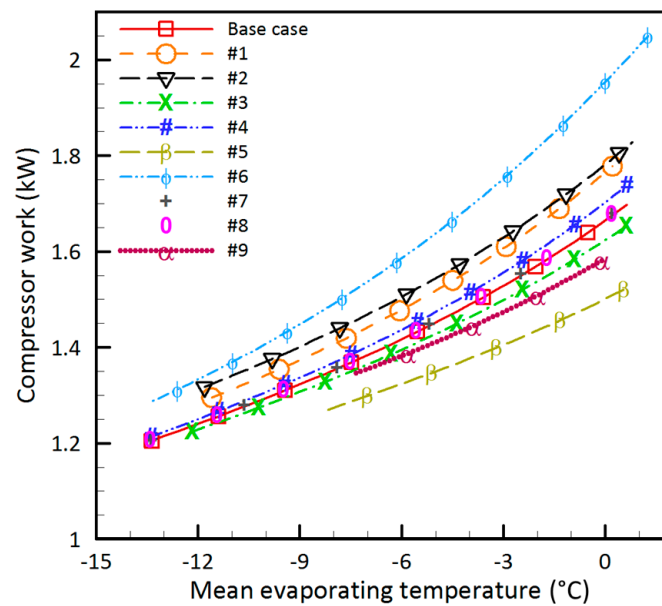


Figure 10. Compressor work (W_{comp}).

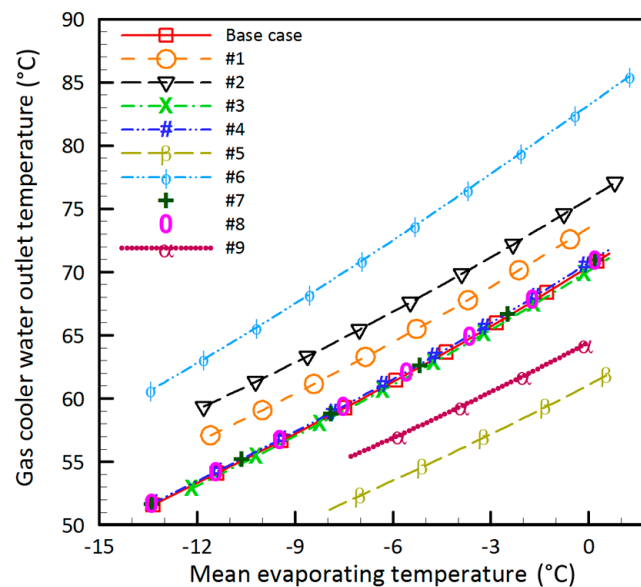


Figure 11. Water outlet temperature (T_{out_water}).

4.4. The Effect of Inlet Water Temperature to the Gas Cooler

Case #2 was designed to investigate the effect of water temperature entering the gas cooler. Increasing the water inlet temperature reduces the COP up to 6% due to the higher discharge pressure and therefore higher compressor work (Figures 7 and 10). In other words, to keep the outlet CO_2 temperature constant, the compressor needs working more (Figure 10) to discharge the fluid at a higher temperature and pressure.

4.5. The Effect of Superheat

The effect of superheat at the suction of the compressor is highlighted by cases #3 and #4. Under given conditions, higher superheat marginally improves the COP. At higher compressor suction temperatures, CO_2 specific volume increases and therefore reduces both the mass flow rate and the

compressor work. With a trivial effect on the gas cooler heating capacity, higher superheat at the compressor suction, slightly improves the COP of the system.

4.6. The Effects of IHE efficiency and the Intermediate Pressure

According to the results of cases #7 and #8, the intermediate pressure and the efficiency of the IHE do not noticeably affect the COP, q_{gc} , water outlet temperature and the total borehole extraction rate.

4.7. The Combined Effect of CO₂ Gas Cooler Outlet Temperature and Water Flow Rate

Cases #1 and #5 (the cases with the highest COP) were coupled (case #9) to investigate the effect of $T_{out_CO_2}$ and \dot{m}_{water} together, on the performance of the system. Here, $T_{out_CO_2}$ and \dot{m}_{water} were changed similar to cases #1 and #5, respectively. Results show a significant improvement in the COP of the system (up to 12% higher than the base case). Gas cooler capacity is also increased by 7.5% compared to the base case. Moreover, as shown in Figure 9, case #9 offers the highest total borehole extraction rate among all cases for evaporating temperatures from $-6\text{ }^{\circ}\text{C}$ to $0\text{ }^{\circ}\text{C}$ (up to 10% at $0\text{ }^{\circ}\text{C}$ compared to the base case). Apparently, proper control over the discharge pressure of the compressor and appropriate design of the gas cooler significantly improve the performance of a DX-CO₂ GSHP.

4.8. Effect of the Number of Boreholes

The effect of the number of boreholes on COP and gas cooler heating capacity is highlighted by cases BC2 and BC4 in Figures 12 and 13, respectively. According to these figures, the system with a lower number of boreholes mainly operates with a lower evaporating temperature. Reducing the number of boreholes results in a smaller heat transfer area inside the ground and a higher CO₂ flow rate in each borehole. Therefore, to satisfy a certain superheat, the system needs to operate at a lower evaporating temperature and this creates a larger temperature difference between the CO₂ and the ground. Eventually, the gas cooler heating capacity is limited in the case with two boreholes. The average heating capacity of the gas cooler in the case with two boreholes is 28% less than the case with four boreholes. A similar phenomenon has been observed experimentally in [37]. Although the flow rate per borehole is reduced by increasing the number of boreholes, the overall thermal resistance of the borehole does not change significantly. The calculated thermal resistances of the base case, four and two boreholes are 0.230, 0.232, and 0.228 [M·K/W], respectively.

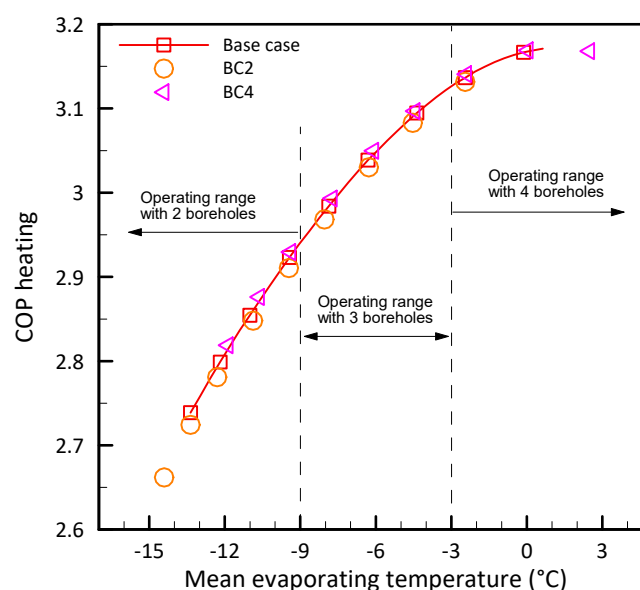


Figure 12. Coefficient of performance ($COP_{heating}$).

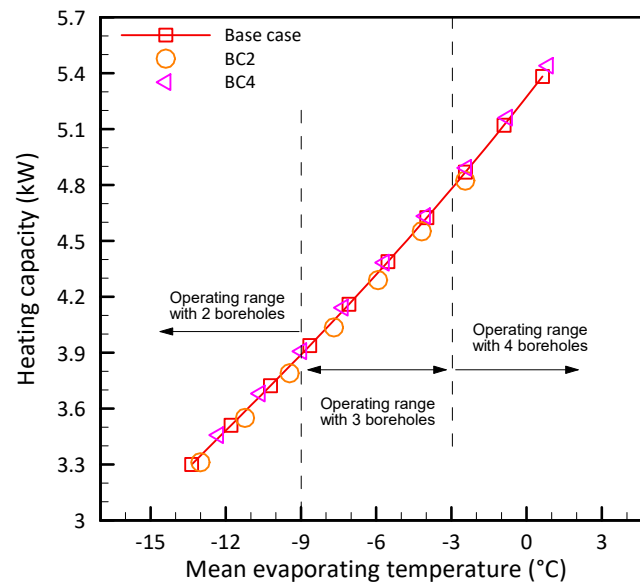


Figure 13. Gas cooler heating capacity (q_{gc}).

As shown in Figures 12 and 13, although the heat pump works at lower evaporating temperatures with fewer boreholes (Figure 5), heat pump performance parameters (COP and heating capacity) follow an identical curve. However, in Figure 14, the difference between the inlet and outlet pressure (pressure drop) of the borehole in BC2, BC4 and the base case is more evident. Negative values in Figure 14 imply that the CO_2 flow pressure gain due to gravity is higher than the acceleration and friction pressure drop. Using two boreholes increases the pressure drop by up to 5 times more than that of the base case at certain evaporating temperatures (e.g., at -3°C). There is a pressure gain in the borehole for BC4 over almost the whole operating range of the system. For BC4 and the base case, the pressure drop decreases as the evaporating pressure increases. However, the opposite behavior is observed from -15°C to -5°C for BC2 (pressure drop increases as the evaporating pressure increases).

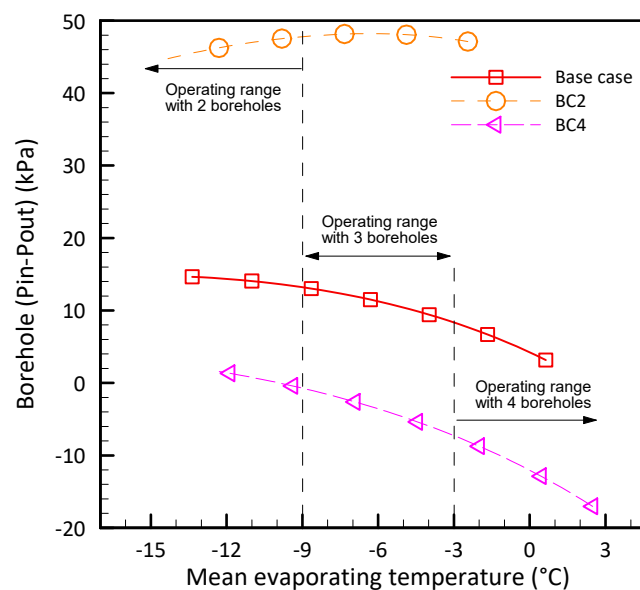


Figure 14. Pressure change in the ground heat exchanger ($P_{in}-P_{out}$).

5. Conclusions

While DX CO₂ GSHP is an energy efficient and environmental friendly option for providing space heating and hot water in buildings, the lack of related technical knowledge of these systems hinders its application in the market. To address this issue, a previously developed theoretical model was modified and validated using experimental results. The experiments were conducted using a test bench built and commissioned at CanmetENERGY research laboratory, Varennes, Canada. A detailed performance analysis of the system was numerically carried out for water heating to identify the important parameters and their effects. Parameters, including the degree of superheat at the compressor suction, inlet water temperature to the gas cooler, CO₂ gas cooler outlet temperature, intermediate pressure, water mass flow rate, IHE efficiency and number of boreholes in the GHE were selected. The effect of these parameters on the COP of the system, heating capacity of the gas cooler, compressor work, discharge pressure, water outlet temperature and total borehole extraction rate was investigated.

Results showed that efficient domestic hot water heating (COP of over 3) with relatively high temperature difference between inlet and outlet of the water tank (30 °C), is achievable using transcritical DX-GSHP systems. However, improper control of some parameters such as gas cooler CO₂ outlet temperature and discharge compressor pressure can degrade the system performance up to 25%. Beside the proper design of the gas cooler, the controlling parameters (e.g., the discharge pressure) need to be set correctly as a base for the application. In addition to the heat capacity improvement of the gas cooler, proper control of the system allows the boreholes to work at their full capacity and eventually improves the performance of the system. Moreover, the size of the ground heat exchanger and the number of active boreholes significantly affect the evaporating temperature and consequently the performance of the system. For instance, the COP of the system dropped to 3.06 from 3.17 after a month of continuous operation in the base case (with three boreholes) of this study. However, after the same period, the COP of scenarios with four and two boreholes dropped to 3.11 and 2.89, respectively.

Acknowledgments: This work was financially supported by the Energy Innovation Program (Natural Resources Canada).

Author Contributions: P.E. conceived and developed the theoretical model. He performed calculations and prepared results. M.B. performed the literature survey and contributed to analyzing results and performing the experiments. A.B. analyzed the data, prepared result discussions and contributed in performing the experiments. As the scientific advisor, Z.A. reviewed the work and proposed valuable suggestions for improvement. All authors contributed in writing the manuscript.

Conflicts of Interest: The authors declare no conflict of interest.

Nomenclature

English Alphabet

$2D$	Shank spacing [cm]
A	Surface Area [m ²]
C_p	Constant Pressure Specific Heat Capacity [kJ/kg/K]
k	Thermal Conductivity [W/m/K]
\dot{m}	Mass Flow Rate [kg/s]
P	Pressure [kPa]
q	Heat transfer rate [kW]
T	Temperature [°C]
U	Heat Transfer Coefficient [W/K/m ²]

Greek Alphabet

ρ	Density [kg/m ³]
ϵ_{IHE}	IHE efficiency

Subscript

gc	Gas Cooler
ID	Inside Diameter
IHE	Internal Heat Exchanger
opt	Optimum
OD	Outside Diameter
in	Inlet
out	Outlet
$comp$	Compressor
sh	Superheat

Abbreviation

COP	Coefficient of Performance
DX	Direct Expansion
GSHP	Ground Source Heat Pump
GHE	Ground heat exchanger
SL	Secondary loop

References

1. Florides, G.; Kalogirou, S. Ground heat exchangers—A review of systems, models and applications. *Renew. Energy* **2007**, *32*, 2461–2478. [[CrossRef](#)]
2. Congedo, P.M.; Colangelo, G.; Starace, G. Simulations of Horizontal Ground Heat Exchangers: A Comparison among Different Configurations. *Appl. Therm. Eng.* **2012**, *33–34*, 24–32. [[CrossRef](#)]
3. Ma, Z.; Xia, L. Model-based Optimization of Ground Source Heat Pump Systems. *Energy Procedia* **2017**, *111*, 12–20. [[CrossRef](#)]
4. Kruse, H.; Russmann, H. Novel CO₂-heat pipe as earth probe for heat pumps without auxiliary pumping energy. In Proceedings of the 8th IHA Heat Pump Conference, Las Vegas, NA, USA, 30 May–2 June 2005; pp. 1–12.
5. Bertsch, S.; Groll, E.A.; Herrick, R.W. Modeling of a CO₂ thermosyphon for a ground source heat pump application. In Proceedings of the 8th IHA Heat Pump Conference, Las Vegas, Nevada, USA, 30 May–2 June 2005; Volume 2, pp. 1–11.
6. EA, F.; GS, W. Earth source heat pumps Characteristics, design, and operation. *IEEE J. Mag. Trans. Am. Inst. Electr. Eng.* **1959**, *77*, 540–551.
7. Mei, V.C.; Baxter, V.D. *Experimental Analysis of Direct Expansion Ground Coupled Heat Pump Systems*; Oak Ridge Natl. Lab.: Oak Ridge, TN, USA, 1991.
8. Johnson, W.S. Field tests of two residential direct exchange geothermal heat pumps/Discussion. *ASHRAE Trans.* **2002**, *108*, 99.
9. Goulburn, J.R.; Fearon, J. Deep ground coil evaporators for heat pumps. *Appl. Energy* **1978**, *4*, 293–313. [[CrossRef](#)]
10. Wang, H.; Zhao, Q.; Wu, J.; Yang, B.; Chen, Z. Experimental investigation on the operation performance of a direct expansion ground source heat pump system for space heating. *Energy Build.* **2013**, *61*, 349–355. [[CrossRef](#)]
11. Beauchamp, B.; Lamarche, L.; Kajl, S. A numerical model of a U-tube vertical ground heat exchanger used as an evaporator. *J. Energy Power Eng.* **2013**, *7*, 237.
12. Fannou, J.C.; Rousseau, C.; Lamarche, L.; Kajl, S. Modeling of a direct expansion geothermal heat pump using artificial neural networks. *Energy Build.* **2014**, *81*, 381–390. [[CrossRef](#)]
13. Fannou, J.-L.C.; Rousseau, C.; Lamarche, L.; Kajl, S. A comparative performance study of a direct expansion geothermal evaporator using R410A and R407C as refrigerant alternatives to R22. *Appl. Therm. Eng.* **2015**, *82*, 306–317. [[CrossRef](#)]
14. Wang, X.; Ma, C.; Lu, Y. An experimental study of a direct expansion ground-coupled heat pump system in heating mode. *Int. J. Energy Res.* **2009**, *33*, 1367–1383. [[CrossRef](#)]
15. Minea, V. Combined radiant floor and forced air heating with direct expansion GSHP in a northern greenhouse. In Proceedings of the 21st International Congress of Refrigeration, Washington, DC, USA, 17–22 August 2003.
16. Goulburn, J.R.; Fearon, J. Domestic heat pump with deep hole ground source evaporator. *Appl. Energy* **1983**, *14*, 99–113. [[CrossRef](#)]
17. Fannou, J.; Rousseau, C.; Lamarche, L.; Stanislaw, K. Experimental analysis of a direct expansion geothermal heat pump in heating mode. *Energy Build.* **2014**, *75*, 290–300. [[CrossRef](#)]
18. Beauchamp, B. Modélisation et Validation Expérimentale D’une Pompe à Chaleur Géothermique à Expansion Directe. Ph.D. Thesis, École de Techno-Logie Supérieure, Montréal, QC, Canada, 2011.
19. Kim, M.; Lee, G.; Baik, Y.-J.; Ra, H.-S. Performance evaluation of geothermal heat pump with direct expansion type vertical ground heat exchanger. *Heat Transf. Eng.* **2015**, *36*, 1046–1052. [[CrossRef](#)]
20. Lenarduzzi, F.J.; Bennett, T.J. Direct-expansion ground-source heat pump with spiral ground coil. Heating mode. *ASHRAE Trans.* **1991**, *1991*, 902–908.
21. Yang, W. Experimental performance analysis of a direct-expansion ground source heat pump in Xiangtan, China. *Energy* **2013**, *59*, 334–339. [[CrossRef](#)]
22. Rousseau, C.; Fannou, J.C.; Lamarche, L.; Ouzzane, M.; Kajl, S. Modeling and experimental validation of a transient direct expansion geothermal heat exchanger. *Geothermics* **2015**, *57*, 95–103. [[CrossRef](#)]

23. Clément, R.; Fannou, J.; Lamarche, L.; Ouzzane, M. Modeling and Analyse of a Direct Expansion Geothermal Heat Pump (DX): Part 1 Modeling of Ground Heat Exchanger. In Proceedings of the 2012 COMSOL Conference, Boston, MA, USA, 3–5 October 2012.
24. Safemazandarani, P.; Edwards, J.A.; Johnson, R.R.; Mohammad-Zadeh, Y. Mathematical modeling of a direct expansion ground-coupled heat pump system. *ASHRAE Trans.* **1990**, *96*, 583–589.
25. Beauchamp, B.; Lamarche, L.; Kaji, S. A dynamic model of a vertical direct expansion ground heat exchanger. In Proceedings of the International Conference Renewable Energies Power Qualification, Valencia, Spain, 28–30 September 2009.
26. Halozan, H.; Rieberer, R. Ground source heat pumps—Overcoming market and technical barriers. *IEA HEAT PUMP Progr.* 2011. 12 pages. Annex 29. Available online: <http://heatpumpingtechnologies.org/publications/ground-source-heat-pumps-overcoming-market-and-technicalbarriers/> (accessed on 24 January 2018).
27. Guo, Y.; Zhang, G.; Zhou, J.; Wu, J.; Shen, W. A techno-economic comparison of a direct expansion ground-source and a secondary loop ground-coupled heat pump system for cooling in a residential building. *Appl. Therm. Eng.* **2012**, *35*, 29–39. [[CrossRef](#)]
28. Hakkaki-fard, A.; Eslami-nejad, P.; Aidoun, Z.; Ouzzane, M. A techno-economic comparison of a direct expansion ground-source and an air-source heat pump system in Canadian cold climates. *Energy* **2015**, *87*, 49–59. [[CrossRef](#)]
29. Gao, Y.; Peng, Y.; Liu, J. Comprehensive Benefit Analysis of Direct Expansion Ground Source Heat Pump System. *Energy Power Eng.* **2013**, *2013*, 76–81. [[CrossRef](#)]
30. Omer, A.M. Direct expansion ground source heat pumps for heating and cooling. *Int. Res. J. Eng.* **2013**, *1*, 27–48.
31. Mastrullo, R.; Mauro, A.W.; Menna, L.; Vanoli, G.P. A model for a borehole heat exchanger working with CO₂. *Energy Procedia* **2014**, *45*, 635–644. [[CrossRef](#)]
32. Eslami-nejad, P.; Ouzzane, M.; Aidoun, Z. Modeling of a two-phase CO₂-filled vertical borehole for geothermal heat pump applications. *Appl. Energy* **2014**, *114*, 611–620. [[CrossRef](#)]
33. Yuefen, G.; Yongzhao, C.; Nan, S. Heat transfer performance of the underground CO₂ pipe in the direct expansion ground source heat pump. *Energy Procedia* **2017**, *105*, 4955–4962. [[CrossRef](#)]
34. Ghazizade-ahsae, H.; Ameri, M. Energy and exergy investigation of a carbon dioxide direct-expansion geothermal heat pump. *Appl. Therm. Eng.* **2018**, *129*, 165–178. [[CrossRef](#)]
35. Austin, B.T.; Sumathy, K. Parametric study on the performance of a direct-expansion geothermal heat pump using carbon dioxide. *Appl. Therm. Eng.* **2011**, *31*, 3774–3782. [[CrossRef](#)]
36. Eslami-nejad, P.; Ouzzane, M.; Aidoun, Z. A quasi-transient model of a transcritical carbon dioxide direct-expansion ground source heat pump for space and water heating. *Appl. Therm. Eng.* **2015**, *91*, 259–269. [[CrossRef](#)]
37. Badache, M.; Ouzzane, M.; Eslami-nejad, P.; Aidoun, Z. Experimental study of a carbon dioxide direct-expansion ground source heat pump (CO₂ DX-GSHP). *Appl. Therm. Eng.* **2017**. [[CrossRef](#)]
38. Hellström, G. Ground Heat Storage, Thermal Analysis of Duct Storage System. Ph.D. Thesis, University of Lund, Lund, Sweden, 1991.
39. Lamarche, L.; Beauchamp, B. A new contribution to the finite line-source model for geothermal boreholes. *Energy Build.* **2007**, *39*, 188–198. [[CrossRef](#)]
40. Lemmon, E.W.; Huber, M.L.; McLinden, M.O. *NIST Standard Reference Database 23: Reference Fluid Thermodynamic and Transport Properties-REFPROP*; Version 9.1, Standard Reference Data Program; National Institute of Standards and Technology: Gaithersburg, MD, USA, 2013.

